

available at [www.sciencedirect.com](http://www.sciencedirect.com)journal homepage: [www.elsevier.com/locate/carbon](http://www.elsevier.com/locate/carbon)

# One-pot synthesis of MnO<sub>2</sub>/graphene/carbon nanotube hybrid by chemical method

Ying Chen <sup>a,b</sup>, Yong Zhang <sup>a</sup>, Dognsheng Geng <sup>a</sup>, Ruying Li <sup>a</sup>, Hanlie Hong <sup>b</sup>,  
Jingzhong Chen <sup>b</sup>, Xueliang Sun <sup>a,\*</sup>

<sup>a</sup> Department of Mechanical & Materials Engineering, Faculty of Engineering, The University of Western Ontario, 1151 Richmond Street, London, Ontario, Canada N6A 3K7

<sup>b</sup> Engineering Research Center of Nano-Geomaterials of Ministry of Education, China University of Geosciences Wuhan, 388 Lumo RD, Wuhan 430074, China

## ARTICLE INFO

### Article history:

Received 15 January 2011

Accepted 10 June 2011

Available online 6 July 2011

## ABSTRACT

A branched hybrid of MnO<sub>2</sub>/graphene/carbon nanotube (CNT) is generated in a one-pot reaction process by chemical method. Some ultrathin MnO<sub>2</sub>/graphene nanosheets, around 5 nm in thickness, are randomly distributed on the CNT surface. Morphology, phase structure, microstructure and vibrational properties of the hybrid were characterized by field emission scanning electron microscope, X-ray diffractometer, high resolution transmission electron microscope and Raman spectrometer. Elemental distribution of the hybrid was determined by energy dispersive X-ray mapping performed in scanning transmission electron microscope mode. The key factor of the formation mechanism is associated with both redox and oxidation–intercalation reactions. Graphene flakes are partly exfoliated from the surface layers of the CNTs, and the redox reaction between KMnO<sub>4</sub> and hydroxyl groups occurs on both sides of these flakes, resulting in the formation of a MnO<sub>2</sub>/graphene/CNT hybrid. Brunauer–Emmett–Teller surface area measurements indicate that the hybrid has over four times the specific surface area of the pristine CNTs.

© 2011 Elsevier Ltd. All rights reserved.

## 1. Introduction

Graphene and carbon nanotubes (CNTs) have driven numerous applications in electronics due to their outstanding physical and chemical properties [1–3]. Benefiting from their superior electrical conductivity, high electrochemical stability, good mechanical properties and high specific surface area, both graphene and CNTs are considered as ideal reinforcing components in fabricating complex nanostructured hybrids and composites, thereby tailoring properties of various nanostructured devices.

Manganese oxide (MnO<sub>2</sub>) is a widely used material featuring low-cost, high energy density, environmental pollution-free and nature abundance [4,5]. Recently, much efforts have

been focused on the synthesis of nanoscale MnO<sub>2</sub>/CNT (graphene or porous carbon) hybrids due to their significant electrochemical applications [6–10], such as supercapacitors and lithium ion batteries. However, there are still some challenge to be overcome such as increase of the mass loading on the surface of substrate, effective control of the thickness of MnO<sub>2</sub> films. Generally, MnO<sub>2</sub> deposits readily form planar nanosheets on flat substrates, resulting in the reduced surface area of substrates and thick MnO<sub>2</sub> layers coating [11]. For MnO<sub>2</sub>/CNT composites, Reddy et al. [10] synthesized the coaxial hybrid of MnO<sub>2</sub> and CNTs leading to enhanced Li storage properties. In their further work, they [12] fabricated Au segmented MnO<sub>2</sub>/CNT coaxial arrays which showed improvement in specific capacitance, energy and power density

\* Corresponding author.

E-mail address: [xsun@eng.uwo.ca](mailto:xsun@eng.uwo.ca) (X. Sun).

0008-6223/\$ - see front matter © 2011 Elsevier Ltd. All rights reserved.

doi:10.1016/j.carbon.2011.06.046

because of their good electrical contacts between electrode and current collector. Lee et al. [13] obtained  $\text{MnO}_2/\text{CNT}$  composite with well-controlled ultrathin  $\text{MnO}_2$  films with an approximate thickness of 5 nm. This value is in agreement with nanoscale  $\text{MnO}_2$  which could provide high specific capacitances. The design and fabrication of  $\text{MnO}_2/\text{CNT}$  composites with three-dimensional multifunctional architectures make the  $\text{MnO}_2$  sheets grow along radial direction from the walls of CNTs, which is another possible way to dissolve mentioned problems [14]. Zhang et al. [15] found that  $\text{MnO}_2$  tends to nucleate at the junctions of CNTs and then grow radically from junctions. These  $\text{MnO}_2$  nanoflowers/CNTs arrays are composite with hierarchical porous structure. Xia et al. [16] pre-treated CNTs with  $\text{KMnO}_4$  in neutral conditions to form small nanocrystals of  $\text{MnO}_2$  on the CNT walls, and then the nanocrystals continuously grew into nanoflaky via a hydrothermal process. The key factor of formation of nanoflaky/CNTs composites is that the nanocrystalline  $\text{MnO}_2$  on walls of CNTs serves as the nucleation site. Using graphene as the carbon support, Yan et al. prepared graphene/ $\text{MnO}_2$  by microwave irradiation. The graphene sheets serve as high conductive support, which provide the large surface for the deposition of nanoscale  $\text{MnO}_2$  particles. Wu et al. [17] mixed  $\text{MnO}_2$  nanowires with graphene sheets by solution-phase assembly. Presence of  $\text{MnO}_2$  nanowires on the surface of graphene prevents the stacking of graphene due to the van der Waals interactions, while on the other hand, the high conductivity of graphene is favorable to improve the dispersion of  $\text{MnO}_2$  nanowires and the electrical conductivity. To the best of our knowledge, controlled synthesis and detailed structural scrutiny of  $\text{MnO}_2/\text{graphene}/\text{CNT}$  ternary hybrid have not been reported yet.

In this paper, we report a versatile chemical reaction process for fabricating a kind of three-dimensional hybrid of  $\text{MnO}_2/\text{graphene}/\text{CNT}$  nanostructures. At the low level of oxidation, oxygen-containing groups increased without  $\text{MnO}_2$  nanocrystallines formed. The defects on the walls of CNTs is favorable to intercalation of  $\text{SO}_4^{2-}$  and peeling off of graphene. Afterwards, the partly exfoliated graphene came from the walls of CNT matrix, with the ultrathin  $\text{MnO}_2$  sheets coating on the surface of graphene sheets instead of CNTs. Via strong van der Waals interaction of the un-exfoliated walls and  $\text{MnO}_2$  film coating on the graphene and CNTs, the petal sheets of  $\text{MnO}_2/\text{graphene}$  could stand on the CNT matrix stably. Careful engineering of hybrid reached over four times the specific surface area of the pristine CNTs.

## 2. Experimental

### 2.1. Synthesis of multi-wall carbon nanotubes

The multi-wall carbon nanotubes (MWCNTs) in this work were synthesized by an aerosol-assisted chemical vapor deposition method (Supplementary data Fig. S1). At the beginning, a porcelain substrate was placed in a quartz tube, in which an argon flow (200 sccm) was passed through to purge the system for 20 min. Then the furnace was heated to 900 °C within 15 min. As soon as the temperature at the center of the furnace reached 900 °C, an aerosol (solution containing 11 g of

ferrocene ( $\text{FeCp}_2$ ) in 500 ml of m-xylene) was generated ultrasonically and carried by mixed gas flow of argon A (40 sccm), hydrogen (60 sccm) and argon B (45 sccm, dilute gas) into the quartz tube, and meanwhile water vapor was introduced into the reactor by another flowing argon (40 sccm) through a water bubbler during the growth period. After 30 min of reaction, the ultrasonic sprayer was turned off and argon A was stopped. Hydrogen, water vapor and argon B flow were kept passing through the reactor until the furnace cooled down to room temperature.

### 2.2. Synthesis of $\text{MnO}_2/\text{graphene}/\text{CNT}$ hybrids

In a typical procedure, MWCNTs (10 mg) were ground with  $\text{KMnO}_4$  (100 mg, Aldrich) crystallites by using a mortar and pestle to a powder mixture. This mixture was then suspended in 10 ml de-ionized (DI) water and stirred at room temperature (22 °C) for different time of 1–12 h. After that, a trace amount of concentrated  $\text{H}_2\text{SO}_4$  (50  $\mu\text{l}$ , Aldrich, 95–98 wt.%) was introduced into the system and the stir continued at room temperature for additional 60 min. Afterwards, the solution was heated in an oil bath at 80 °C for 60 min. The reaction mixture was then removed from the heat source, and poured into 500 ml of DI water to cool down and dilute. The solution was filtered over a polytetrafluoroethylene membrane (0.22  $\mu\text{m}$  pore size, Aldrich), and the remaining solid was washed repeatedly with DI water for several times.

### 2.3. Sample characterization

Morphology of the hybrid was characterized by field emission scanning electron microscope (FESEM, Hitachi S-4800). Phase structure of the hybrid was characterized by Bruker D8 micro X-ray diffraction (XRD), operating at 40 kV and 40 mA, with  $\text{Cu K}\alpha$  radiation ( $\lambda = 0.15418$  nm). High resolution investigation of the hybrid was performed with transmission electron microscope/scanning transmission electron microscope (TEM/STEM, JEOL 2010F) equipped with an Oxford INCA Pentafet spectrometer (Oxford Instruments, Abingdon, Oxfordshire, UK). The acceleration voltage was 200 keV. Energy dispersive X-ray mapping (EDX) was performed in STEM mode with a probe size of 1 nm. Raman spectra were collected using Raman Rxn1-785 spectrometer (Kaiser Optical Systems, Inc.) Brunauer–Emmett–Teller (BET) surface area was measured by  $\text{N}_2$  physisorption at 77 K using a Micromeritics ASAP 2010. Fourier transform-infrared (FT-IR) measurements were carried out by the KBr method using a Nicolet 6700 FT-IR spectrometer. FT-IR spectra were recorded in the transmittance mode over the range of 500–4000  $\text{cm}^{-1}$  by averaging 16 scans at a resolution of 4  $\text{cm}^{-1}$ .

## 3. Results and discussion

Fig. 1A and C shows FESEM images of the hybrid, with the morphology of reticular and curved petal-like walls on the carbon nanotubes with originally smooth surface over the entire longitudinal length. Fig. 1B and D depict corresponding TEM images of inherent structure of the petals-tube hybrid, displaying a long-range array of transparent petal-like sheets

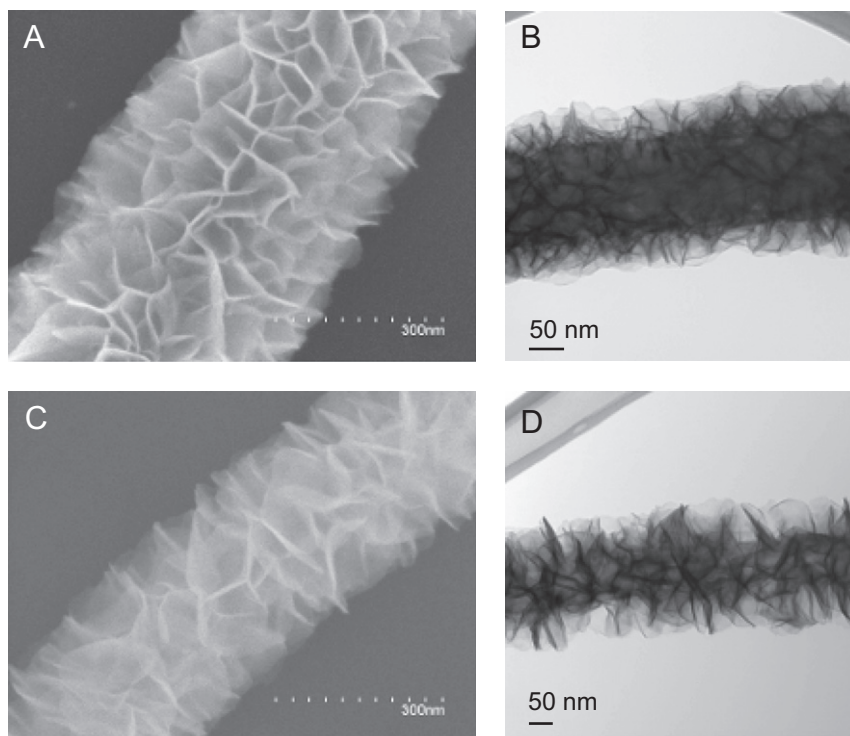


Fig. 1 – (A–D) SEM and TEM characterization of a representative  $\text{MnO}_2$ /graphene/CNT hybrid.

attached upon the sidewalls of the inner nanotubes with the size of  $\sim 280$  nm. Interfacial profiles between the petals and the tube can be well distinguished. A BET surface area test shows that specific surface area of the hybrid is  $143 \text{ m}^2 \text{ g}^{-1}$ ,

presenting a over four times the specific surface area of the pristine carbon nanotubes ( $32 \text{ m}^2 \text{ g}^{-1}$ ).

We used XRD analysis to determine the phase structure of the hybrid Fig. 2A. An evident peak at the  $2\theta$  value of about

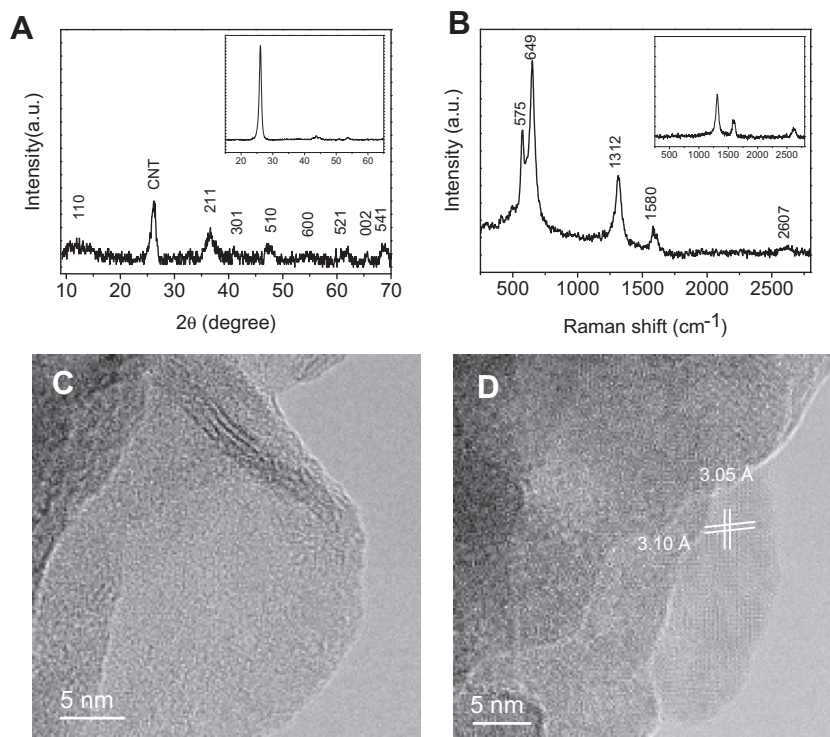


Fig. 2 – (A) XRD patterns of pristine CNTs (inset) and the hybrid. (B) Raman spectra of pristine CNTs (inset) and the hybrid. (C) High-resolution TEM (HRTEM) image obtained from a curved edge of the hybrid. (D) HRTEM image of a single petal-like sheet.

26.05° is consistent with (002) crystal plane of graphite. Other characteristic peaks with marked crystal faces can be assigned to the tetragonal phase of  $\alpha$ -type  $\text{MnO}_2$  (JCPDS 44-0141) [18,19]. We also used Raman spectroscopy to investigate vibrational properties of the hybrid Fig. 2(B). Intensity ratio of D to G band ( $I_d/I_g$ ) increases accordingly from 1.53 to 2.77 with the oxidation reaction progress, indicating the enhanced level of disorder within the product and the formation of  $\text{sp}^3$  carbon by functionalization. In addition, two sharp, low frequency bands at about 575 and 649  $\text{cm}^{-1}$  can be used to characterize the tunnel species of  $\alpha$ -type  $\text{MnO}_2$  materials, which are commonly attributed to the Mn–O stretching vibration in the basal plane of  $\text{MnO}_6$  sheet, and the symmetric stretching vibration Mn–O of  $\text{MnO}_6$  groups [20,21]. Moreover, the edge of a representative petal-like sheet Fig. 2C was ascertained by high-resolution TEM, showing the thickness below 5 nm and counted with four layers or less considering the stacking possibility of two or more curving sheets. Two lattice fringes with the spacing 0.305 and 0.310 nm Fig. 2D can be indexed as (130) and (3 $\bar{1}$ 0) crystal planes of  $\alpha$ -type  $\text{MnO}_2$ , respectively, which is consistent with XRD and Raman observations.

The energy dispersive X-ray mapping performed in scanning transmission electron microscope mode is demonstrated in Fig. 3. Fig. 3A shows a TEM image of a representative segment of the hybrid, a bare carbon nanotube segment is indicated in the circle area of the picture. Fig. 3B–D shows elemental distribution of C, Mn and O in the hybrid. Besides strong signal of the CNT inner core, the mapping results indicate that the distribution of C, Mn and O elements is homogeneous throughout the petal-like nanosheets, implying that the nanosheets are composed of manganese oxide and C. The mapping results in the circle area reveal that the bare

nanotube is composed of only carbon without manganese oxide coatings.

Previous reports have indicated that two kinds of structures can be obtained in a CNT- $\text{KMnO}_4$  system under different conditions. If strong acid was introduced into the system, CNTs were cleaved in the longitudinal direction and unzipped to graphene ribbons under stronger oxidized environment without forming nanostructured  $\text{MnO}_2$  [22]. If the level of oxidation is weaker, the  $\text{MnO}_2$  nanocrystallines will nucleate on the defective sites of CNTs and then grow into the sheets coating on the CNT surface [16]. Based on the above characterization, it seems that our results are different from the two cases. Commonly, two kinds of reactions may take place in a CNT- $\text{KMnO}_4$  system. One reaction (A) is oxidation–intercalation–exfoliation [16,23]. Carbon nanotubes are considered as the graphite curved along one dimension with stacks of graphene. Depending on the  $\pi$ -conjugated network and van der Waals interactions of carbon atoms, the crystal structure of CNTs is stable. When the oxygen groups are introduced on the CNT walls, spacing of external layers is increased. The graphene sheets can be cleaved from the walls of carbon nanotube during an oxidation–intercalation process, which was demonstrated by Kosynkin et al. [22]. Although the strong  $\pi$ – $\pi$  bonds exist in the walls of the MWCNTs, the surface oxidation could disrupt the  $\pi$ -conjugated network and liberate graphene sheets from the nanotube. The open degree depends on the level of oxidation. If the MWCNTs were treated under weaker acidic conditions, the walls would be partly exfoliated. The un-exfoliated parts of the walls could link the graphene to the MWCNTs.

Another reaction process is oxidation–reduction [24,25]. When the redox reaction is occurred between carbon and  $\text{KMnO}_4$  in acid solution, it is as follows:

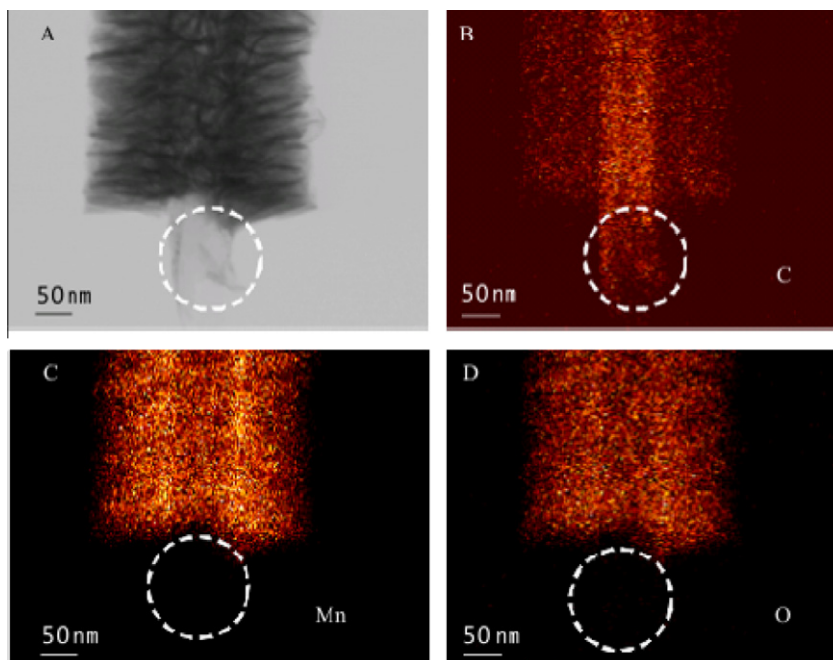


Fig. 3 – (A) TEM image of a representative hybrid segment with and without petal sheets surrounding the CNT. (B–D) STEM-EDX mapping results for C, Mn and O elements.



In this reaction, the graphene sheets serve as the sacrificial reductant and convert the  $\text{Mn}^{+7}$  to  $\text{Mn}^{+4}$  and thereby nanostructured  $\text{MnO}_2$  are produced. As Yan et al. [11] reported, synthesis of  $\text{MnO}_2$  nanocrystals was promoted through the rapid nucleation on the graphene surface under microwave irradiation with short reaction time, and the  $\text{MnO}_2$  particles dispersed at the edges of graphene layers. In our experiments, the high ratio of  $\text{KMnO}_4$  to CNTs promoted the oxidation of the CNT walls instead of nucleation of  $\text{MnO}_2$ , which is different from the previous research about the mechanism of three-dimensional  $\text{MnO}_2/\text{CNT}$  nanocomposites by Xia et al. [16]. In order to explore the role of  $\text{KMnO}_4$  and  $\text{H}_2\text{SO}_4$  during the growth of hybrid, some control experiments were carried out.

Fig. 4 shows the TEM images and Fourier transform infrared (FT-IR) spectroscopy of CNTs treated only with  $\text{KMnO}_4$  before heat (Fig. 4a), and images of the CNTs treated with  $\text{KMnO}_4$  and different amount of  $\text{H}_2\text{SO}_4$  (Fig. 4c–e). Comparing

to the pristine CNTs, as shown in Fig. 4a, the CNT walls kept smooth without any  $\text{MnO}_2$  nanocrystals observed when the nanotubes were only treated by  $\text{KMnO}_4$ . And we used FT-IR spectroscopy to track the functional groups on the surface of  $\text{KMnO}_4$ -treated MWCNTs (Fig. 4b). The spectra of the transformed MWCNTs illustrate the presence of the  $\text{C}=\text{O}$  ( $\nu_{\text{C}=\text{O}}$  at  $1640\text{ cm}^{-1}$ ),  $\text{C}-\text{OH}$  ( $\nu_{\text{C}-\text{OH}}$  at  $1380\text{ cm}^{-1}$ ) and the  $\text{COOH}/\text{OH}$  ( $\nu_{\text{COOH}/\text{OH}}$  at  $3400\text{ cm}^{-1}$ ) [22]. With incremental exposure of the MWCNTs to  $\text{KMnO}_4$ , these characteristic peaks stepwisely increase and broaden except the peak at  $1380\text{ cm}^{-1}$ , the  $\text{C}-\text{O}-\text{C}$  ( $\nu_{\text{C}-\text{O}-\text{C}}$  at  $3400\text{ cm}^{-1}$ ) stretch appears in sample a–c, indicating an increase number of carboxyl and hydroxyl functionalities. All these functional group changes reveal that oxidation degree of the final MWCNTs is remarkably dependent on the  $\text{KMnO}_4$  pre-treatment time. There is no observation of nanoscale  $\text{MnO}_2$ .

In order to obtain further information of initial growth of  $\text{MnO}_2$  and the exfoliation from CNTs, detailed high resolution TEM studies were carried out.

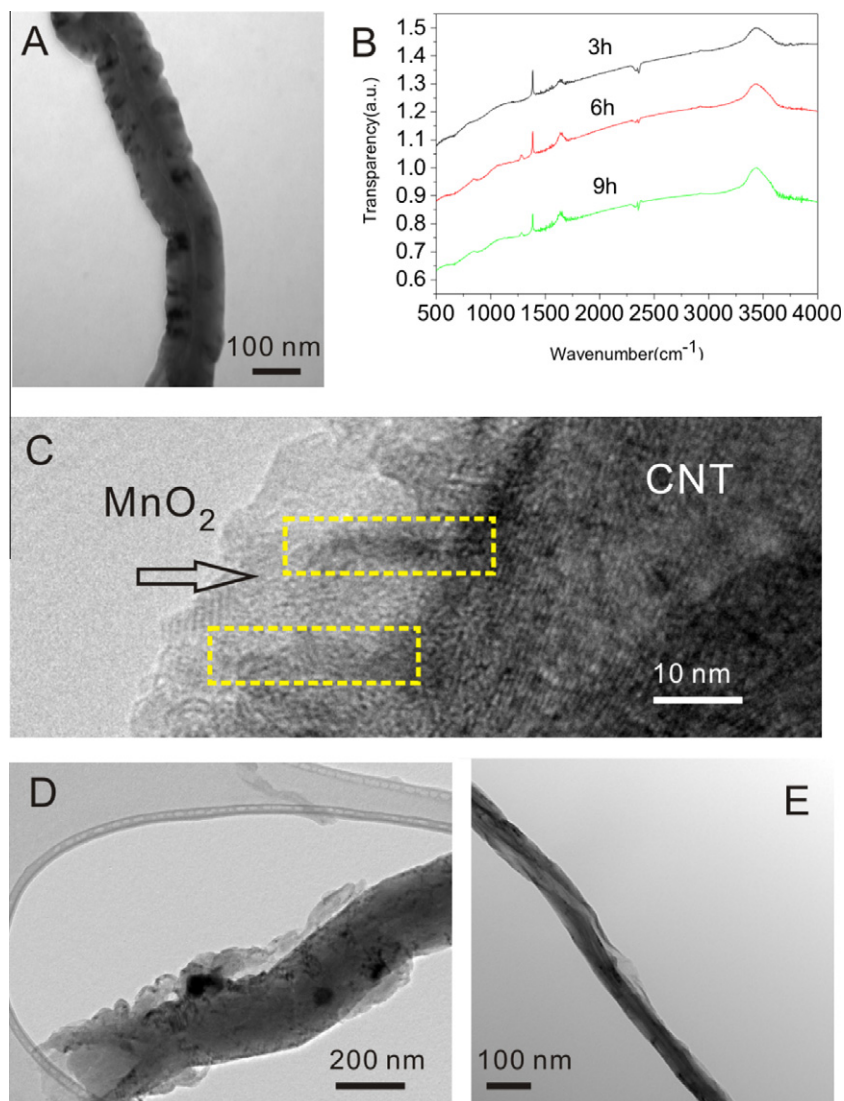


Fig. 4 – (A) TEM image of CNTs treated with  $\text{KMnO}_4$  in water for 9 h; (B) FT-IR spectrum of CNTs treated with  $\text{KMnO}_4$  in water for 3, 6, 9 h, respectively, TEM image of the CNT treated with  $\text{KMnO}_4$  and, (C) 50  $\mu\text{l}$ ; (D) 2 ml; (E) 10 ml  $\text{H}_2\text{SO}_4$ .

Fig. 4c shows the TEM image of the initial growth of the hybrid based on the CNTs treated with  $\text{KMnO}_4$  and low amount of  $\text{H}_2\text{SO}_4$  (50  $\mu\text{l}$ ), same as the conditions of the sample shown in Fig. 1. The areas marked by the dotted border indicate that some petals were (about 10 nm long) partly exfoliated from the CNT, and the petals were surrounded by  $\text{MnO}_2$ . When high amount of  $\text{H}_2\text{SO}_4$  was used, the longitudinal unzipping of the nanotubes instead of  $\text{MnO}_2$  deposition was observed as shown in Fig. 4d (2 ml of  $\text{H}_2\text{SO}_4$ ), and Fig. 4e (10 ml of  $\text{H}_2\text{SO}_4$ ).

Based on the above results, it indicates that the structure control of the hybrid in our work is expected to be dominated by a competition between the two reactions of oxidation–intercalation–exfoliation and oxidation–reduction processes, and the growth of  $\text{MnO}_2$ /graphene/CNTs hybrid is proposed in this work by carefully controlling the growth parameters.

To get further insight into the structure of the hybrid, we ever adopted a general method to remove the excess of permanganate and  $\text{MnO}_2$ , sufficient amount of hydrogen peroxide ( $\text{H}_2\text{O}_2$ ) and a solution of HCl in water (1:10 v/v dilution from commercial concentrated HCl) were added and then the samples were washed by large amount of distilled water repeatedly. Fig. 5a shows TEM image of the samples after reduction, revealing that the spatial architecture of the sample is satisfyingly maintained. We used Raman technique to investigate the vibrational properties of the treated samples. Comparing to the samples without treatment, the Raman result shows the obvious change of characteristic peaks which belong to the  $\text{MnO}_2$ . The peak located at  $649\text{ cm}^{-1}$  disappears and the density of peak at  $575\text{ cm}^{-1}$  is decreased, indicating

that the large amount of  $\text{MnO}_2$  nanocrystals were destroyed after treatment. Furthermore, the density of the multi-band peaks around  $2607\text{ cm}^{-1}$  (2D) are increased obviously, which is consistent with the multi-layer feature of graphene because of decrease of  $\text{MnO}_2$  amount. This is also supported by the SEM–EDX results. The EDX reflects the mass loading of  $\text{MnO}_2$  from 33% down to 5% (the range is 5–10%). It is still difficult to observe the details of their microstructure directly owing to the complexity of samples which are consisted of CNTs,  $\text{MnO}_2$  and graphene-like carbon. Due to the coating of residual  $\text{MnO}_2$  on the graphene-like petal sheet, and the 3-D architecture is stable even under stir or ultrasonic treatment. The presence of  $\text{MnO}_2$  limited the characterization of the quality of the graphene sheet directly, even after the treatment of the samples with HCl and  $\text{H}_2\text{O}_2$  to destroy the large amount of  $\text{MnO}_2$  nanocrystals. Due to the non-uniform exfoliation of CNT walls and consumption of exfoliated graphene, the final state of graphene sheets can be: (1) completely exfoliated graphene sheets; (2) partly exfoliated graphene sheets attached on the CNT; (3) a sacrificial reductant and exhausted.

Besides dose of  $\text{H}_2\text{SO}_4$ , the morphology of  $\text{MnO}_2$  of the composites also strongly depended on reaction temperature and reaction time. Generally, higher temperature or longer reaction time would favor the gain of petal sheets formed. Keeping other optimized conditions the same, morphology and size of the carbon/ $\text{MnO}_2$  sheets were able to be readily modulated by adjusting each one of the three factors. Here dependence of the hybrid morphology on the temperature is taken as the example. Fig. S3 shows low and high magnification SEM images of the hybrids processed at 40, 60 and 80  $^\circ\text{C}$ ,

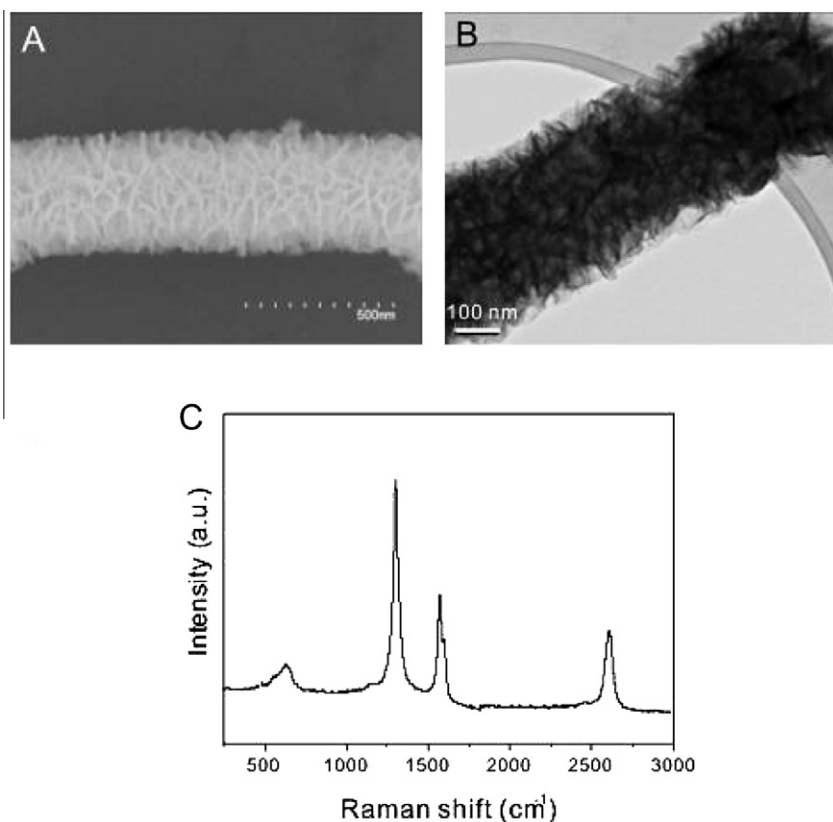


Fig. 5 – (A, B) SEM and TEM images of, (C) Raman spectrum of samples after HCl and  $\text{H}_2\text{O}_2$  treated.

respectively, demonstrating stepwise growth of the petal sheets. At low temperature of 40 °C, the CNTs surface still remains relatively smooth except some corrugated structures. With the increase of the temperature, corrugated structure becomes entangled network and finally develops into the cross-linked petal-like structure on the CNT surface. The amount of  $\text{H}_2\text{SO}_4$  had to be controlled as low as 1 ml, otherwise carbon/ $\text{MnO}_2$  sheets would be peeled off from CNTs (Fig. S4). Moreover, the CNTs would be unzipped in the longitudinal direction under large amount of  $\text{H}_2\text{SO}_4$ . The treatment time of  $\text{H}_2\text{SO}_4$  also needs to be carefully tuned to make the oxidation process more controllable. Long treatment time in the presence of  $\text{H}_2\text{SO}_4$  could lead to the break of the hybrids into short segments (Fig. S5).

Depending on preparation processes, different carbon materials may exhibit different microstructures and properties, such as defects on surface, specific surface area and electrical conductivity. Therefore, we tried some usual carbon materials with the identical process, including graphene sheets, commercial MWCNTs with different diameters, flake graphite and spherical-like acetylene black which seem to be formed by graphene sheets in the scroll geometry. For the growth of the  $\text{MnO}_2$  on the graphene sheets (Fig. S6), both flat and flower like structure can be found due to the difference among the local surface conditions of the graphene sheets. This indicates that  $\text{MnO}_2$  is expected to be uniformly deposited on the graphene nanosheets depending on the

experimental conditions and quality of the graphene sheets. The morphologies of the received products grown on commercial MWCNTs and flake graphite substrates are similar to those grown from the MWCNTs in this work. We could observe the presence of a densely crossed array of the free-standing nanosheets with different size and curved shape in our samples with the commercial CNTs, and flake graphite inside (Figs. S7 and S8). However, in the case for acetylene black, the original carbon source exhausted and resultant hierarchical structure with hollow center was obtained. The low resolution SEM and TEM images (Fig. S9) of as-received samples show uniform changes of their morphologies and high yields. Besides few of the separate samples, most of which was still aggregated, being determined by the separate particles or aggregated chains of starting materials. TEM-EDX of single petal sheet shows the obtained sample is composed of four elements, namely C, K, Mn and O. This is different from the previous research on  $\text{KMnO}_4$ -acetylene system [8], in which just  $\text{MnO}_2$  nanostructures were obtained and the carbon source was released by generating  $\text{CO}_2$  gas completely, revealing that large amount of carbon atom are composited with  $\text{MnO}_2$  during the experimental process.

Thus, we suggest the following mechanism of the  $\text{MnO}_2$ /graphene/CNT ternary hybrid demonstrating in the schematic as shown in Fig. 6: (1) on the initial stage,  $\text{KMnO}_4$  is mixed with CNTs in a neutral condition. The large amount of  $\text{KMnO}_4$  acts as a “weak oxidizing agent” due to much less

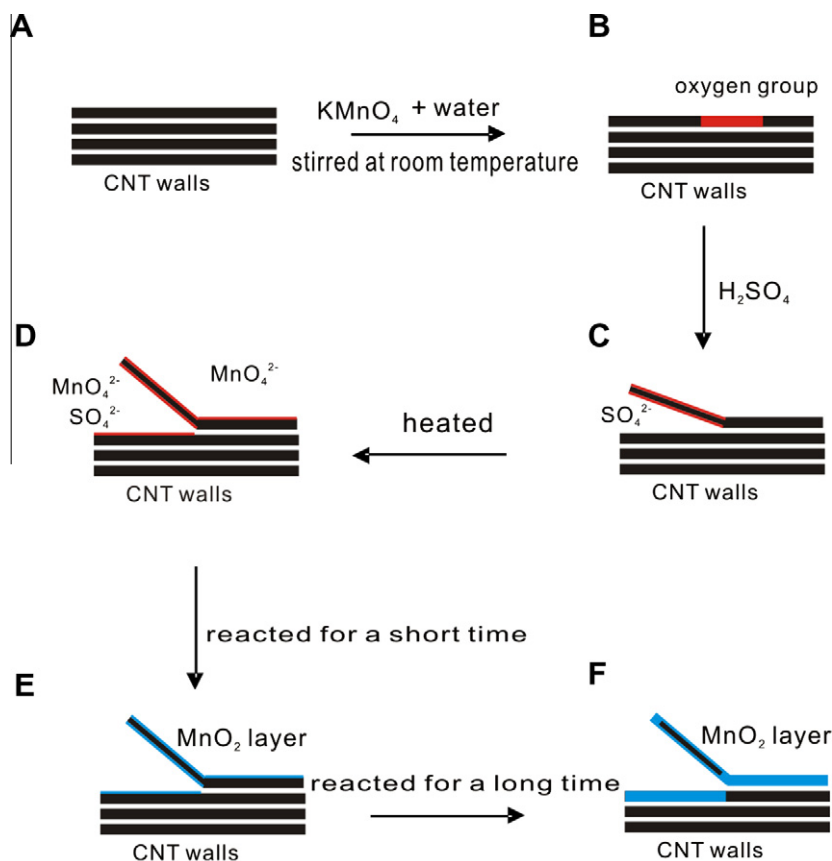


Fig. 6 – Schematic diagram of a proposed mechanism for the evolution steps from CNTs to  $\text{MnO}_2$ /graphene/CNT hybrid.

positive electrode potential of the agent in a neutral condition than that in an acid ambient [26]. During the slow oxidation process, oxygen-containing groups would anchor spontaneously on the carbon nanotubes, especially on defective sites of the nanotube surface. However, the reduction of  $\text{MnO}_4^-$  by water is unfavorable. (2) When  $\text{H}_2\text{SO}_4$  is introduced into the system,  $\text{KMnO}_4$  in the acidic ambient leads to higher oxidation degree of the CNTs, which links those oxidized sites into curved epoxy chains (also called fault lines) and finally to various patterns [27]. Gradually,  $\text{MnO}_4^-$  ions are absorbed and precipitated on the oxidized location through the interactions between remained  $\text{KMnO}_4$  and hydroxyl groups. The redox reaction is controlled kinetically at a very slow rate. (3) When the solution mixture is heated, oxidation degree of the nanotube sidewalls is significantly enhanced and  $\text{SO}_4^{2-}$  ions intercalate into the sidewalls preferentially along the “pattern” initiated by the epoxy chains. Since graphene flakes are partly exfoliated, reduction of large amount of  $\text{Mn}^{7+}$  to  $\text{MnO}^{4+}$  happens at both sides of the partly exfoliated graphene flakes, preventing the deposition of  $\text{MnO}_2$  on the CNT surface.

#### 4. Conclusions

The high yield and uniform hybrid of  $\text{MnO}_2$ /graphene/CNT is synthesized by a multi-oxidation process. By adjusting the level of the oxidization, the  $\pi$ - $\pi$  stacking of surface layers in pristine CNTs could be disrupted partly, which favors both intercalation and redox reactions happened on the graphene surface. The un-disrupted segment made sure the graphene remain on the CNT matrix stably, and final formed 3-D architecture with  $\text{MnO}_2$  coating. This readily controlled process by coordinating the involved parameters makes it possible for the production of hybrid with well-defined structure in an industrial scale. The resultant structure can find great potential applications in developing various nanodevices in the field of electrochemical energy, catalysis and microelectronics. The present work may open a new door towards nano-electronics and other realms where hybridized structures are required.

#### Acknowledgements

This work is supported by NSERC, the CRC Program, CFI, ORF, ERA, UWO and the foundation of Engineering Research Center of Nano-Geomaterials of Ministry of Education (No. 201006). Y. Chen thanks the China Scholarship Council.

#### Appendix A. Supplementary data

Supplementary data associated with this article can be found, in the online version, at doi:10.1016/j.carbon.2011.06.046.

#### REFERENCE

[1] Novoselov KS, Geim AK, Morozov SV, Jiang D, Katsnelson MI, Grigorieva IV, et al. Two-dimensional gas of massless Dirac fermions in graphene. *Nature* 2005;438(7065):197–200.

- [2] Wang XR, Ouyang YJ, Li XL, Wang HL, Guo J, Dai HJ. Room-temperature all-semiconducting sub-10-nm graphene nanoribbon field-effect transistors. *Phys Rev Lett* 2008;100(20):2068031–4.
- [3] Iijima S. Helical microtubules of graphitic carbon. *Nature* 1991;354(6348):56–8.
- [4] Komaba S, Ogata A, Tsuchikawa T. Enhanced supercapacitive behaviors of birnessite. *Electrochem Commun* 2008;10(10):1435–7.
- [5] Ma SB, Nam KW, Yoon WS, Yang XQ, Ahn KY, Oh KH, et al. Electrochemical properties of manganese oxide coated onto carbon nanotubes for energy-storage applications. *J Power Sour* 2008;178(1):483–9.
- [6] Chabre Y, Pannetier J. Structural and electrochemical properties of the proton gamma- $\text{MnO}_2$  system. *Prog Solid State Chem* 1995;23(1):1–130.
- [7] Hou Y, Cheng YW, Hobson T, Liu J. Design and synthesis of hierarchical  $\text{MnO}_2$  nanospheres/carbon nanotubes/ conducting polymer ternary composite for high performance electrochemical electrodes. *Nano Lett* 2010;10(7):2727–27233.
- [8] Chen W, Fan ZL, Gu L, Bao XH, Wang CL. Enhanced capacitance of manganese oxide via confinement inside carbon nanotubes. *Chem Commun* 2010;46(22):3905–7.
- [9] Fischer AE, Pettigrew KA, Rolison DR, Stroud RM, Long JW. Incorporation of homogeneous, nanoscale  $\text{MnO}_2$  within ultraporous carbon structures via self-limiting electroless deposition: implications for electrochemical capacitors. *Nano Lett* 2007;7(2):281–6.
- [10] Reddy ALM, Shaijumon MM, Gowda SR, Ajayan PM. Coaxial  $\text{MnO}_2$ /carbon nanotube array electrodes for high-performance lithium batteries. *Nano Lett* 2009;9(3):1002–6.
- [11] Yan J, Fan ZJ, Wei T, Qian WZ, Zhang ML, Wei F. Fast and reversible surface redox reaction of graphene- $\text{MnO}_2$  composites as supercapacitor electrodes. *Carbon* 2010;48(13):3825–33.
- [12] Reddy ALM, Shaijumon MM, Gowda SR, Ajayan PM. Multisegmented Au- $\text{MnO}_2$ /carbon nanotube hybrid coaxial arrays for high-power supercapacitor applications. *J Phys Chem C* 2010;114(1):658–63.
- [13] Lee SW, Kim J, Chen S, Hammond PT, Shao-Horn Y. Carbon nanotube/manganese oxide ultrathin film electrodes for electrochemical capacitors. *ACS Nano* 2010;4(7):3889–96.
- [14] Rolison DR, Long RW, Lytle JC, Fischer AE, Rhodes CP, McEvoy TM, et al. Multifunctional 3D nanoarchitectures for energy storage and conversion. *Chem Soc Rev* 2009;38(1):226–52.
- [15] Zhang H, Cao GP, Wang ZY, Yang YS, Shi ZJ, Gu ZN. Growth of manganese oxide nanoflowers on vertically-aligned carbon nanotube arrays for high-rate electrochemical capacitive energy storage. *Nano Lett* 2008;8(9):2664–8.
- [16] Xia H, Lai MO, Lu L. Nanoflaky  $\text{MnO}_2$ /carbon nanotube nanocomposites as anode materials for lithium-ion batteries. *J Mater Chem* 2010;20(33):6896–902.
- [17] Wu ZS, Ren WC, Wang DW, Li F, Liu BL, Cheng HM. High-energy  $\text{MnO}_2$  nanowire/graphene and graphene asymmetric electrochemical capacitors. *ACS Nano* 2010;4(10):5835–42.
- [18] Luo J, Zhu HT, Fan HM, Liang JK, Shi HL, Rao GH, et al. Synthesis of single-crystal tetragonal alpha- $\text{MnO}_2$  nanotubes. *J Phys Chem C* 2008;112(33):12594–8.
- [19] Xiao W, Wang DL, Lou XW. Shape-controlled synthesis of  $\text{MnO}_2$  nanostructures with enhanced electrocatalytic activity for oxygen reduction. *J Phys Chem C* 2010;114(3):1694–700.
- [20] Julien C, Massot M. Spectroscopic studies of the local structure in positive electrodes for lithium batteries. *Phys Chem Chem Phys* 2002;4(17):4226–35.
- [21] Julien C, Massot M, Baddour-Hadjean M, Franger S, Bach S, Pereira-Ramos JP. Raman spectra of birnessite manganese dioxides. *Solid State Ion* 2003;159(3–4):345–56.

- [22] Kosynkin DV, Higginbotham AL, Sinitskii A, Lomeda JR, Dimiev A, Price BK, et al. Longitudinal unzipping of carbon nanotubes to form graphene nanoribbons. *Nature* 2009;458(7240):872–6.
- [23] Higginbotham AL, Kosynkin DV, Sinitskii A, Sun ZZ, Tour JM. Lower-defect graphene oxide nanoribbons from multiwalled carbon nanotubes. *ACS Nano* 2010;4(4):2059–69.
- [24] Zhang GX, Sun SH, Ionescu MI, Liu H, Zhong Y, Li RY, et al. Controlled growth/patterning of Ni nanohoneycombs on various desired substrates. *Langmuir* 2010;26(6):4346–50.
- [25] Choi HC, Shim M, Bangsaruntip S, Dai HJ. Spontaneous reduction of metal ions on the sidewalls of carbon nanotubes. *J Am Chem Soc* 2002;124(31):9058–9.
- [26] Chang KC, Li LX, Gloyna EF. Supercritical water oxidation of acetic-acid by 419 potassium-permanganate. *J Hazard Mater* 1993;33(1):51–62.
- [27] Li JL, Kudin KN, McAllister MJ, Prud'homme RK, Aksay IA, Car R. Oxygen-driven unzipping of graphitic materials. *Phys Rev Lett* 2006;96(17):1761011–4.